Tuning the Organic Electrochemical Transistor (OECT) Threshold Voltage with Monomer Blends

Downloaded from: https://research.chalmers.se, 2026-09-08 03:20 UTC

Citation for the original published paper (version of record):
Priyadarshini, D., Li, C., Rilemark, R. et al (2025). Tuning the Organic Electrochemical Transistor (OECT) Threshold Voltage with Monomer Blends. Advanced Electronic Materials, 11(17). http://dx.doi.org/10.1002/aelm.202400681

N.B. When citing this work, cite the original published paper.

research.chalmers.se offers the possibility of retrieving research publications produced at Chalmers University of Technology. It covers all kind of research output: articles, dissertations, conference papers, reports etc. since 2004. research.chalmers.se is administrated and maintained by Chalmers Library

(article starts on next page)

ADVANCED ELECTRONIC MATERIALS Open Access
www.advelectronicmat.de

Tuning the Organic Electrochemical Transistor (OECT) Threshold Voltage with Monomer Blends

*Diana Priyadarshini, Changbai Li, Rebecka Rilemark, Tobias Abrahamsson, Mary J. Donahue, Xenofon Strakosas, Fredrik Ek, Roger Olsson, Chiara Musumeci, Simone Fabiano, Magnus Berggren, Eva Olsson, Daniel T. Simon, and Jennifer Y. Gerasimov**

A novel approach is introduced to modulate the threshold voltage of organic electrochemical transistors (OECTs) that are fabricated by electropolymerizing the channel material between the source and drain electrodes. To achieve this, we adjust the ratio of two water-soluble tri-thiophene monomers, which share the same backbone, but present either anionic or zwitterionic sidechains, during channel formation. This approach allows for a continuous modulation of both the electropolymerization onset potential and the native doping state of the film. We attribute the effect of monomer blends displaying properties that are a weighted average of their components to the formation of nanoscale monomer aggregates that have a uniform internal charge density. Through an investigation of monomer aggregation behavior, polymer film growth, and device properties of OECTs fabricated by electropolymerization, we highlight the importance of monomer aggregation in the electropolymerization of conducting polymers. The ability to tune both electropolymerization onset and the OECT threshold voltage has significant implications for the development of more complex circuits for integrated neuromorphic computing, biosensing, and bioelectronic systems.

1. Introduction

Increasingly complex analog systems implementing organic electrochemical transistors (OECTs) necessitate the ability to fine-tune the minimum gate voltage that is required to form a conducting path, i.e., their threshold voltage. Threshold voltage is a key device specification to be considered when designing integrated circuits for sensors, amplifiers, and logic gates. The capacity to precisely tune the threshold voltage can be exploited to optimize sensitivity and reduce power consumption, as well as avoid undesirable reaction pathways.[1,2] To date, the threshold voltage of an OECT has been tuned by changing the electrochemical potential of the gate electrode by various methods, such as changing the gate electrolyte,[3] chemical doping of polymer deposited at the gate,[4] using a secondary gate,[5] changing the channel length,[6] and even changing the device operating temperature.[7] While copolymerization of monomers with different conjugated backbones by electrochemical methods has been demonstrated in the past, the properties of the resulting copolymers are unpredictable,[8] do not follow a given trend,[9] and have never been used to fabricate OECTs.

D. Priyadarshini, C. Li, T. Abrahamsson, M. J. Donahue, X. Strakosas, C. Musumeci, S. Fabiano, M. Berggren, D. T. Simon, J. Y. Gerasimov
Laboratory of Organic Electronics
Department of Science and Technology
Linköping University
Norrköping 60174, Sweden
E-mail: jennifer.gerasimov@liu.se

R. Rilemark, E. Olsson
Department of Physics
Chalmers University of Technology
Gothenburg 41296, Sweden

The ORCID identification number(s) for the author(s) of this article can be found under https://doi.org/10.1002/aelm.202400681

© 2024 The Author(s). Advanced Electronic Materials published by Wiley-VCH GmbH. This is an open access article under the terms of the Creative Commons Attribution License, which permits use, distribution and reproduction in any medium, provided the original work is properly cited.

DOI: 10.1002/aelm.202400681

F. Ek, R. Olsson
Chemical Biology & Therapeutics
Department of Experimental Medical Science
Lund University
Lund 22184, Sweden

R. Olsson
Department of Chemistry and Molecular Biology
University of Gothenburg
Gothenburg 40530, Sweden

M. Berggren
Wallenberg Initiative Materials Science for Sustainability
Department of Science and Technology
Linköping University
Norrköping 60174, Sweden

2199160x, 2025, 17, Downloaded from https://advanced.onlinelibrary.wiley.com/doi/10.1002/aelm.202400681 by Statens Beredning, Wiley Online Library on [30/10/2025]. See the Terms and Conditions (https://onlinelibrary.wiley.com/terms-and-conditions) on Wiley Online Library for rules of use; OA articles are governed by the applicable Creative Commons License

In this context, a simplified material-based method of adjusting the threshold voltage by copolymerizing water-soluble tri-thiophene monomers with a common conjugated backbone (2,5-bis(2,3-dihydrothieno[3,4-b][1,4]dioxin-5-yl)thiophene, (i.e., EDOT-thiophene-EDOT, abbreviated as ETE), but with differing sidechains is introduced. The two ETE structural variants used are functionalized on the central 3-thiopheneethanol unit with either a butanesulfonic acid sodium salt sidechain (ETE-S) or a phosphocholine sidechain (ETE-PC). Previously, the sidechain was shown to affect the oxidation potential of the monomer as well as act as an intrinsic dopant for the polymer, which directly influences the threshold voltage of an OECT produced by electropolymerization.[10] Here, it is reported that when the monomers are mixed in different ratios, they do not retain their individual properties, but rather the values of oxidation potential and threshold voltage are a weighted average of the components. Since ETE-S and -PC are inherently surfactants that form nanoscale aggregates in aqueous solutions,[11] it is hypothesized that by blending the monomers, the intrinsic doping level of the OECT channel materials can be adjusted continuously. A continuously tunable threshold voltage is expected to greatly facilitate the construction of more complex circuits for integrated neuromorphic computing, biosensing, and bioelectronic systems.

2. Results and Discussion

Monomer blends of ETE-S and ETE-PC were evaluated at a range of relative concentrations (ETE-S 100%, 75%, 50%, 25%, and 0%) to investigate the aggregation behavior of the monomers, the properties of the films formed by electropolymerization, along with the characteristics of the OECT devices fabricated by electropolymerization of these monomer blends.

2.1. Characterizing the Aggregation Behavior of the Monomers

The ETE-S and ETE-PC monomers used in this work are inherently surfactants, and previous reports have shown that they form nanoscale aggregates in aqueous solutions.[11] To verify that the monomer blends investigated herein form uniform aggregates that incorporate both components at the given blend ratios, the photophysical, electrochemical, and structural properties of the monomers and blends are evaluated, and the results are presented in **Figure 1**.

One way to assess the internal structure of the aggregates is to observe the photophysical properties of the monomers. Close spacing of the ETE cores within an aggregate allows for energy transfer between neighboring monomers that can be observed as a new red-shifted low-intensity peak in the corresponding absorbance spectrum (Figure 1a,b), and as the evolution of a fluorescence peak when the excitation wavelength (450 nm) falls within the range of this red-shifted peak in the absorbance spectrum (Figure 1c; Figure S1, Supporting Information).[11] It should be noted that the presence of the additional peaks in the absorbance and fluorescence spectra does not quantify the aggregates, but rather provides information about the organization of monomers within the aggregates.[11] All samples (ETE-S, ETE-PC, and their blends) show an absorbance peak at 350 nm corresponding to their monomer state, and a low-intensity peak centered at 475 nm. While the intensity of the peak at 350 nm does not correlate with the ETE-S:ETE-PC ratio, the absorbance at 450 nm is the lowest for samples containing predominantly ETE-PC and the highest for samples containing predominantly ETE-S, with the 50:50 blend roughly in the middle. This is consistent with previously reported behavior of ETE-S and ETE-PC, each at a concentration of 0.001 M in DI water, where monomer peaks are centered near 350 nm, while aggregation and π–π stacking interactions cause the formation of another absorbance band ≈460 nm, which is more pronounced for ETE-S than for ETE-PC.[11] This trend of more pronounced π–π stacking within aggregates of ETE-S compared to ETE-PC is even more seen in Figure 1c, where excitation at 450 nm produces continuously decreasing peak emission values with increasing percentages of ETE-PC. In contrast, excitation at 350 nm produces an emission peak that increases in intensity with increasing ETE-PC concentrations. Interestingly, the emission peak at an excitation of 350 nm is mostly unaltered below an ETE-PC ratio of 50%, which potentially indicates another form of energy transfer that is not probed in these spectra. These results suggest that ETE-S aggregates in a way that promotes π–π stacking, resulting in more linear aggregates and more efficient energy transfer between neighboring monomers, while ETE-PC forms amorphous aggregates and continuously breaks up the structure of ETE-S aggregates when introduced.

While spectroscopic characterization provides valuable insight into the internal morphology of ETE-X aggregates, it is insufficient in determining whether the aggregates are composed of both ETE-S and ETE-PC at nominal proportions, or if homogeneous aggregates (containing molecules with the same sidechain) are formed in different proportions. To resolve this ambiguity, the oxidation potential of the monomer blends is evaluated by CV (Figure 1d,e). As reported previously, ETE-S and ETE–PC are oxidized at different potentials due to the differences in the charge density provided by the sidechain.[10] Relative to an Ag/AgCl reference, it is observed that ETE-S is oxidized at 0.35 V while ETE-PC is oxidized at 0.48 V when a gold QCM-D crystal is used as the working electrode and a platinum plate is used as a counter electrode. If homogeneous aggregates were present in different proportions, distinct oxidation peaks for ETE-S and ETE-PC would be expected in the blended samples. Instead, there is a smooth transition in the oxidation potential of the blends between the two values, indicating a uniform distribution of ETE-S and ETE-PC within the aggregates. There is evidence of two peaks only in the 25% ETE-S sample, which potentially indicates that there is a limit past which phase segregation begins to occur in the monomer aggregates.

Structural characterization of the ETE-X aggregates is performed via LPTEM (**Figure 2**a–c), DLS (Figure 2d,e), and SEM (Figure S2, Supporting Information). LPTEM and SEM imaging are performed on 0.005 M solutions of pure ETE-S, pure ETE-PC, and ETE-S:PC 50:50, since the working concentration of 0.001 M did not provide sufficient contrast to be imaged using the available microscope. Both LPTEM (dark features) and SEM (bright features) show the presence of aggregated monomers distributed in the solution. Pure ETE-S solution shows aggregates whose shape can be described as thin platelets or discs, with thickness ranging from 15 to 30 nm, and diameter ranging from 50 to 300 nm. Pure ETE-PC solution shows circular aggregates of ≈30 to 70 nm in diameter, as well as elongated fiber-like

 © 2024 The Author(s). Advanced Electronic Materials published by Wiley-VCH GmbH

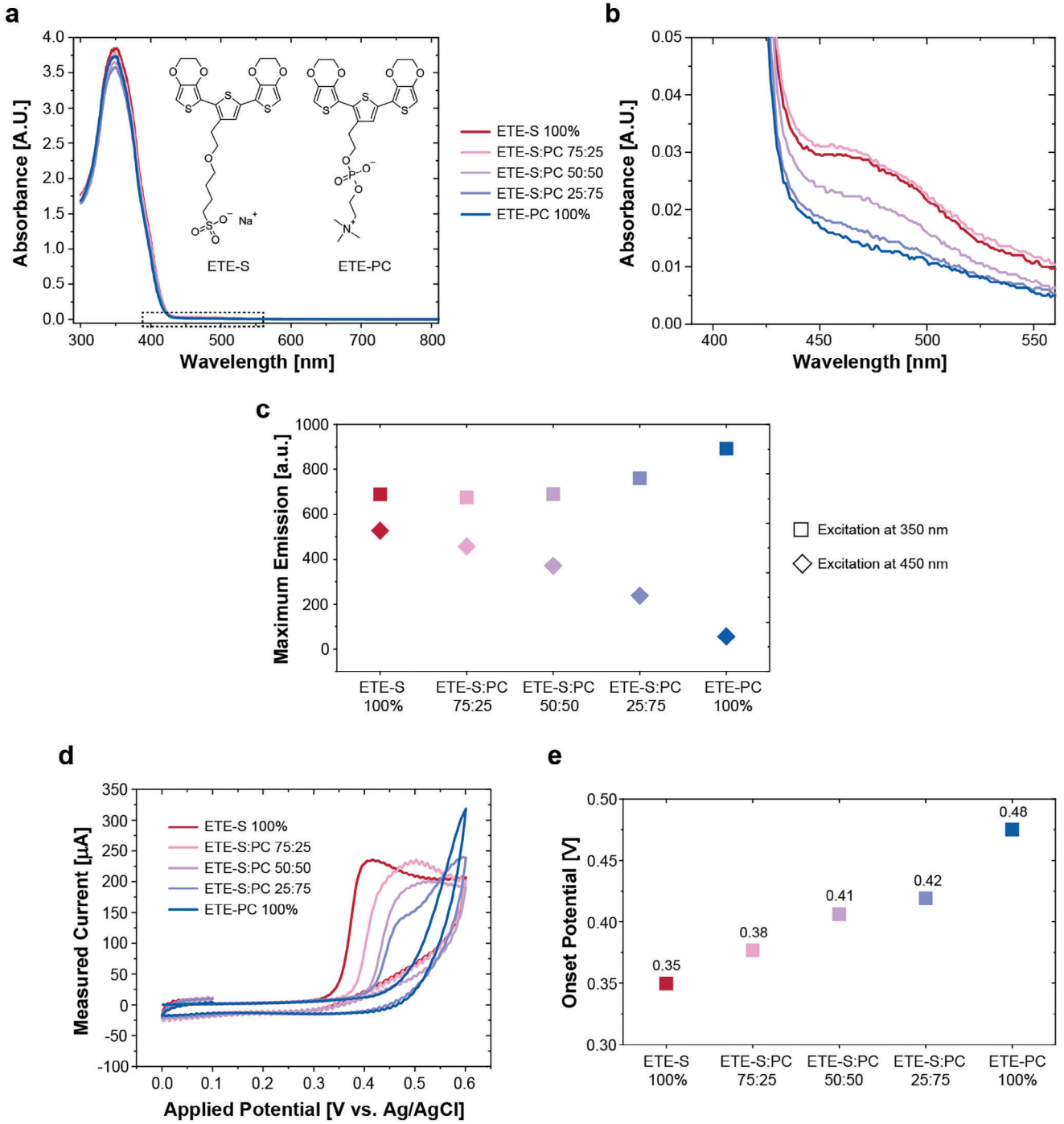

Figure 1. a) Absorbance spectra for the five monomer solutions, along with an inset showing the chemical structures of anionic ETE-S and zwitterionic ETE-PC molecules; b) magnified view (dotted rectangle) of the red-shifted peak of each absorbance spectrum; c) maximum peak intensity of the emission spectrum for each monomer sample upon excitation at 350 and 450 nm; d) first scan cycle of the cyclic voltammogram for the five monomer samples (Au working electrode, Pt counter electrode, single junction Ag/AgCl reference electrode, scan rate 0.1 V s^{-1}) and the e) corresponding electropolymerization onset potential for the five samples.

clusters, which are 15–30 nm wide and 50–150 nm long. These fiber-like clusters resemble a line of round clusters, like a string of pearls. The ETE-S:PC 50:50 solution, however, contains a mixture of round clusters having a diameter in the 30–50 nm range, along with elongated structures similar in shape and size to the fibrous clusters in the ETE-PC 100% solution.

Evaluation by DLS (Figure 2d,e) provides a complementary estimation of the size distribution of the monomer aggregates in pure ETE-S, pure ETE-PC, and ETE-S:PC 50:50 solutions. Both

© 2024 The Author(s). Advanced Electronic Materials published by Wiley-VCH GmbH

2199160x, 2025, 17, Downloaded from https://advanced.onlinelibrary.wiley.com/doi/10.1002/aelm.202400681 by Statens Beredning, Wiley Online Library on [30/10/2025]. See the Terms and Conditions (https://onlinelibrary.wiley.com/terms-and-conditions) on Wiley Online Library for rules of use; OA articles are governed by the applicable Creative Commons License

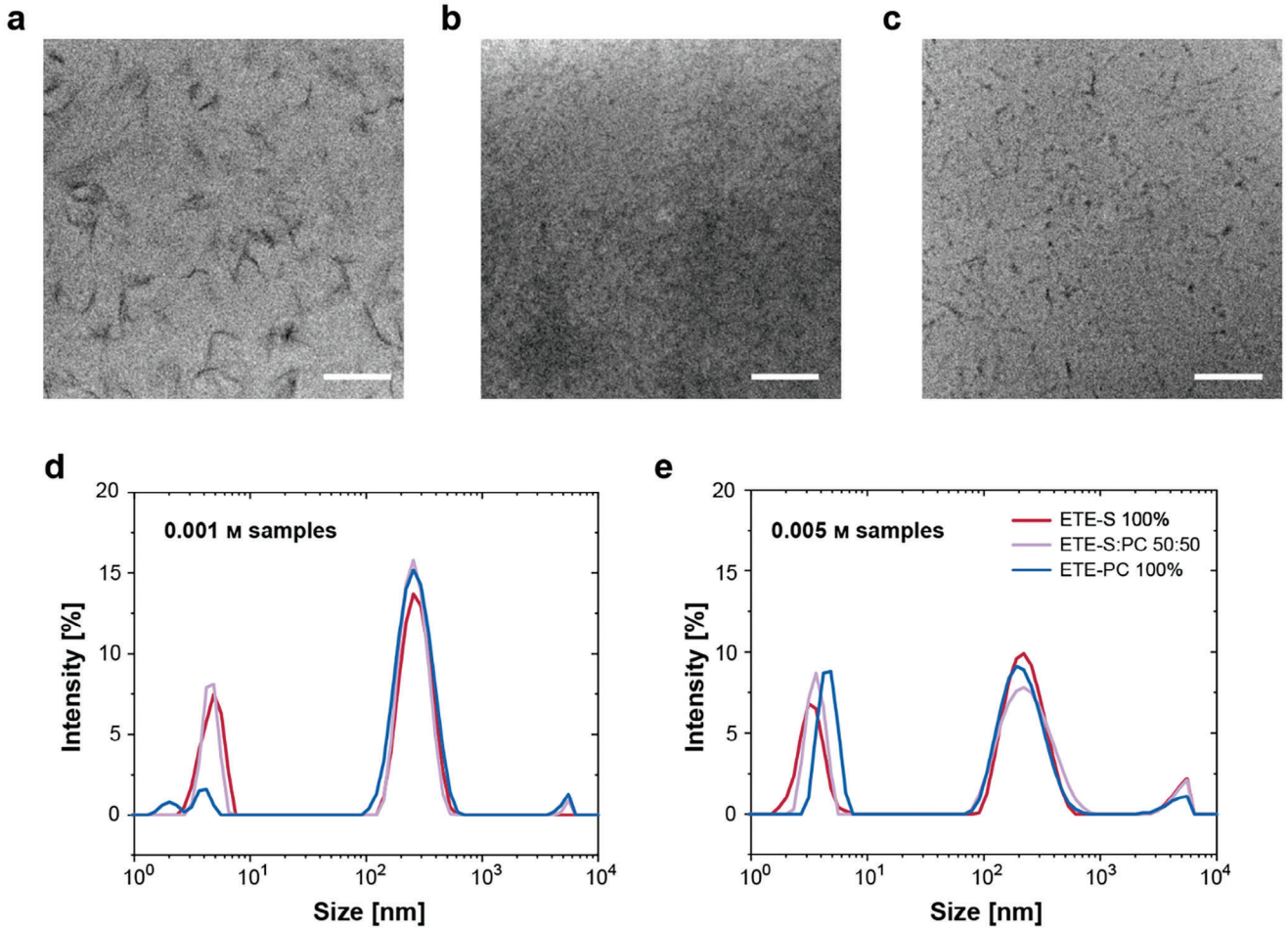

Figure 2. Bright-field LPTEM images of a) ETE-S 100%, b) ETE-S:PC 50:50, and c) ETE-PC 100% monomer solutions, each at a concentration of 0.005 M in 0.01 M NaCl electrolyte (0.01 M concentration too low to visualize in the instrument), scale bar 500 nm; average size distribution for the pure ETE-S and ETE-PC along with ETE-S:PC 50:50 samples, each at a concentration of d) 0.001 M and e) 0.005 M, in 0.01 M NaCl electrolyte.

the working concentration of 0.001 M and the higher concentration of 0.005 M are measured to verify the similarity of the aggregates at these concentrations. DLS measurements of the three samples reveal the presence of what appears to be two distinct populations of particles, one with an apparent hydrodynamic diameter in the range of 3–4 nm and a population with a larger apparent diameter of 190–255 nm (assuming spherical particles). A similar bimodal distribution has been reported for DLS measurements of gold nanorods,[12–14] and silver-spiked stars.[15] The two distributions are variously reported to correspond to either the different dimensions (diameter and length) of the nanorods or to the rotational and translational diffusion constants of the particles. Since the presence of a small radius (0.5–3 nm) population has also been reported for slightly elongated gold nanoparticles with an average radius of 65 nm,[14] the latter explanation is presumed to be more valid. Thus, the polydisperse distribution observed in the DLS results is determined to be consistent with the evaluation of LPTEM images in both the approximate size of the aggregates and the anisotropic geometry, as rotational diffusion can only be observed for non-spherical particles.

2.2. In Situ Electropolymerization and Film Properties

The growth of polymer films formed by in situ electropolymerization of ETE-S, ETE-PC, and their blends is evaluated using EQCM-D (**Figure 3**). During an in situ electropolymerization experiment, a constant flow of 0.01 M NaCl electrolyte is applied to establish a baseline, after which the monomer sample is introduced at 360 s, which causes a minimal shift in f_3 and D_3 values (≈−10 Hz and 0.1 ppm, respectively), corresponding to monomer adhesion to the Au surface of the EQCM-D sensor. At 540 s, an electrodeposition protocol, consisting of three potential steps that are identical to those used in OECT fabrication, is initiated. While the monomer is still flowing within the module, a constant voltage of −0.05 V is first applied for 60 s. Then, a potential corresponding to the electropolymerization onset potential that is determined for each sample (Figure 1d,e), with an additional offset of +0.2 V, is applied for 60 s. Electropolymerization is performed at different potentials to account for differences in the thermodynamic barriers to oxidation between the samples. Finally, a potential of −0.05 V is applied for 60 s. Monomer flow is stopped at ≈900 s, whereupon the capacitance of the films is

© 2024 The Author(s). Advanced Electronic Materials published by Wiley-VCH GmbH

2199160x, 2025, 17, Downloaded from https://advanced.onlinelibrary.wiley.com/doi/10.1002/aelm.202400681 by Statens Beredning, Wiley Online Library on [30/10/2025]. See the Terms and Conditions (https://onlinelibrary.wiley.com/terms-and-conditions) on Wiley Online Library for rules of use; OA articles are governed by the applicable Creative Commons License

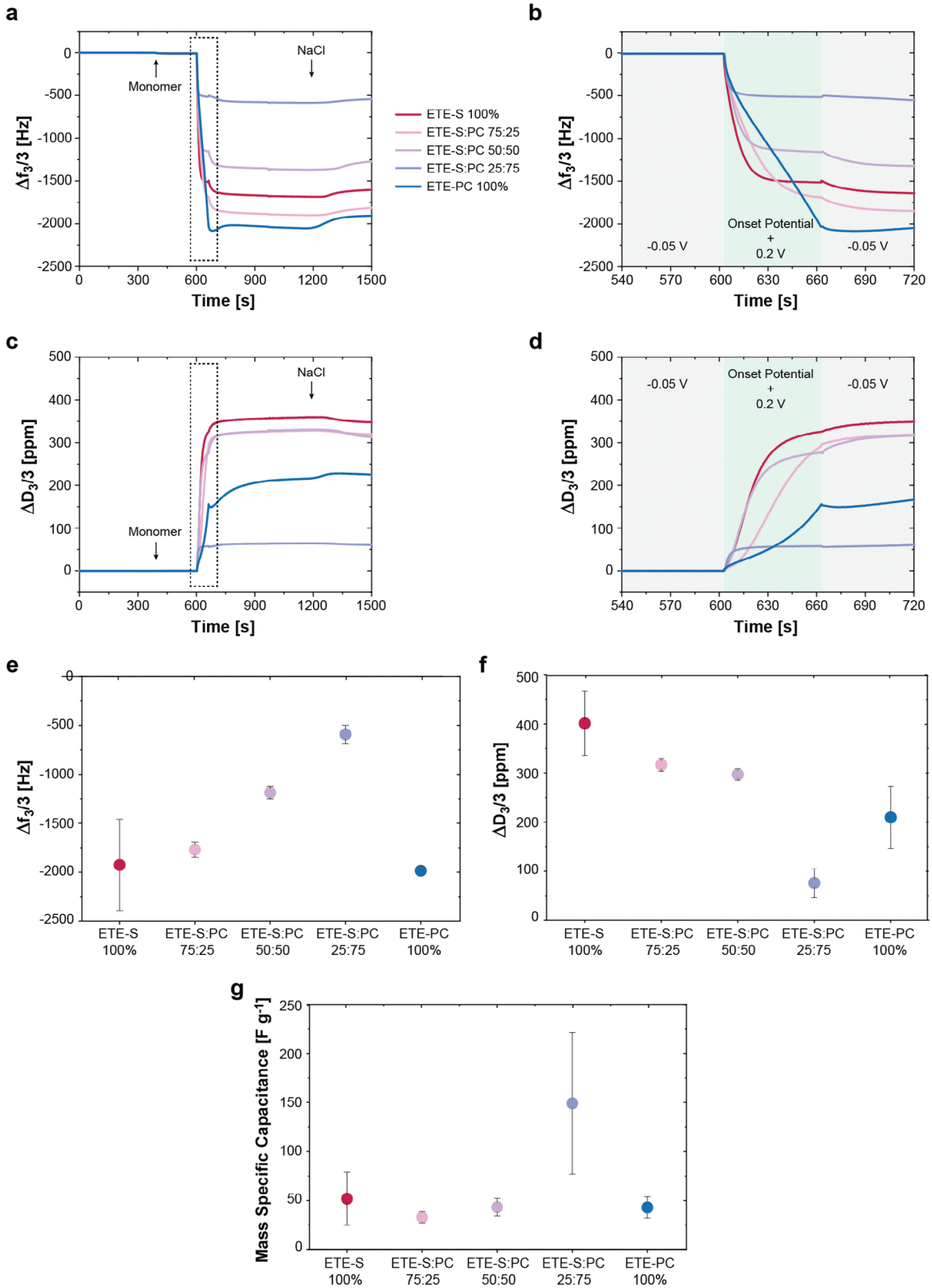

Figure 3. Third overtone-normalized a) frequency and c) dissipation shifts for the five samples over time, along with b,d) corresponding magnified views (dotted rectangle) during the three-step CA procedure for 60 s each, as indicated by the two gray (−0.05 V applied) and one green (onset + 0.2 V applied) rectangles; average values for the e) frequency and f) dissipation shifts of the third overtone at the end of EQCM-D measurement (after electrolyte rinse), along with g) mass-normalized capacitance, calculated using CV and EQCM-D data at ≈960 s (before electrolyte rinse); error bars represent standard deviation, $n = 3$.

 © 2024 The Author(s). Advanced Electronic Materials published by Wiley-VCH GmbH

2199160x, 2025, 17, Downloaded from https://advanced.onlinelibrary.wiley.com/doi/10.1002/aelm.202400681 by Statens Beredning, Wiley Online Library on [30/10/2025]. See the Terms and Conditions (https://onlinelibrary.wiley.com/terms-and-conditions) on Wiley Online Library for rules of use; OA articles are governed by the applicable Creative Commons License

measured by a CV measurement (Figure S5, Supporting Information). The flow is restarted with 0.01 M NaCl at ≈1200 s to rinse off poorly adhered portions of the electropolymerized film.

Representative frequency and dissipation data, corresponding to the third overtone for the five monomer samples, are shown in Figure 3a–d. Negative frequency shifts are indicative of an increase in the hydrated mass adsorbed to the sensor surface while positive dissipation shifts indicate an increase in viscoelasticity of the adsorbed material.[16,17] Some notable differences are apparent in the electropolymerization kinetics between the ETE-S-containing samples and the pure ETE-PC sample. The initial deposition rate is more rapid for all ETE-S samples, after which they show signs of saturation within the 60 s electropolymerization window. In contrast, the rate of ETE-PC film growth is relatively constant within the timeframe of electropolymerization. These effects are presumed to be caused by the negative charge on the sulfonate sidechain of ETE-S. When the potential is initially applied to the QCM-D sensor, the sulfonate promotes electromigration of the aggregates toward the surface of the positively charged electrode. However, once the polymer layer passivates the gold substrate, the surface charge repels additional aggregates from approaching within a distance that allows for efficient electron transfer at the electrode-polymer interface. When the potential is stepped back to −0.05 V after electropolymerization, all samples that contain ETE-S exhibit a negative shift in frequency, which is attributed to the swelling of the film due to the removal of the positive potential at the electrode.

The average magnitude ($n = 3$) of the f_3 and D_3 shifts after the NaCl rinse at the end of each measurement is shown in Figure 3e,f. While the f_3 shifts of pure ETE-S and pure ETE-PC are not statistically different (P-value 0.8382, which is ≫0.05),[18] the ETE-PC film is clearly more rigid than ETE-S due to its lower $\Delta D/\Delta f$ ratio[19,20] (Figure S4a, Supporting Information). The blends, however, follow a clear trend where the increasing proportion of ETE-PC exhibits a decrease in the magnitude of measured Δf_3 values and an increase in the percentage of the mass removed during the final rinse with NaCl (Figure S4c, Supporting Information). For all samples, the proportion of mass removed in the rinse correlates with layer thickness, suggesting that the mass is being removed from the surface of the film in contact with the electrolyte. This loss in mass is attributed to the removal of residual monomer that is entrapped in the film during electropolymerization.

Capacitance values are extracted from the fifth cycle of the corresponding CV plot (Figure S5, Supporting Information) by integrating between 0 and +0.11 V, a region with negligible contributions from redox peaks or other parasitic contributions.[21,22] Specific mass values are extracted from corresponding QCM-D data by applying Kelvin–Voigt viscoelastic modeling ('broadfit' feature; overtones 3, 5, 7, and 9; 5 mm of the active sensing spot diameter)[16,23,24] and are used to calculate the gravimetric capacitance values for the five samples (Figure 3g). The capacitance values are relatively uniform across the samples, with the exception of the 25% ETE-S sample, which has the highest standard deviation, the lowest adsorbed mass (Table S1, Supporting Information), and the highest fraction of material removed during the rinse with NaCl (Figure S4, Supporting Information). It is impossible to conclusively deduce the cause of this phenomenon based on the available data, but one possible explanation is that there is less entrapped monomer within the 25% ETE-S layer due to its comparatively lower thickness (corresponding to lower mass). The increased values of specific capacitance can then be attributed to the reduced presence of electrically insulating monomer aggregates within the bulk of the material.

To determine the qualitative morphology and quantitative topography information of the polymer surfaces, electropolymerized films from the EQCM-D measurement are evaluated by AFM (**Figure 4**). The surface roughness values determined using these images are listed in **Table 1**.

A higher percentage of ETE-S compared to ETE-PC in the mixture seems to result in similar morphology and roughness in the film. The ETE-PC 100% has the smoothest surface of all the five samples. The ETE-S:PC 25:75 mix, however, shows the most uneven feature distribution and roughest surface, which may be evidence of non-uniformity caused by phase separation that was seen in the CV of the monomer.

2.3. OECT Characterization

While QCM-D and AFM are useful in evaluating the properties of a film grown on an electrode, several additional factors contribute to the effectiveness of OECT formation by electropolymerization. Previous study showed that surface treatment of the SiO_2 substrate by an amine-terminated silane (APTES) is essential to control the interactions between the substrate and ETE-S and ETE-PC monomers, thereby pre-concentrating the monomer at the surface and promoting the lateral growth of the polymer film.[10] Without APTES pre-treatment, the lateral growth of the PETE-S polymer encounters the same saturation limits observed in QCM-D experiments (Figure 3), extending only several hundreds of nanometers away from the electrode. Conveniently, both ETE-S and ETE-PC spread well on APTES-modified surfaces.[10]

To evaluate the process of channel formation, OECT devices are fabricated by electropolymerizing ETE-S, ETE-PC, and each of the polymer blends, between a set of Cr-backed Au source and drain electrodes patterned on an APTES-modified silicon wafer (**Figure 5a**). The active electrode area is defined by an opening in the SU-8 photoresist. Monomer solution is deposited directly onto a device consisting of 46 independently addressed channels (W = 100 µm, L = 10 µm) and a larger gold electrode (1 × 2 mm^2) inside a PDMS well. The potential of electropolymerization onset is determined separately for each of the five monomer samples from the first cycle of the corresponding cyclic voltammogram, obtained using the larger Au electrode as the working electrode and an Ag/AgCl pellet as the reference electrode in a two-electrode configuration. The onset potential determined by CV, with an additional offset of +0.2 V, is applied for 60 s (Figure S6a, Supporting Information) between the OECT source contact and an Ag/AgCl pellet shorted with the OECT drain contact to electropolymerize the monomer sample and form a polymer channel between the source and drain electrodes. A potential of −0.05 V is also applied for a period of 60 s before and after channel growth (Figure 5b) to evaluate channel conductance at a potential below the polymerization threshold.

The kinetics of the current change during OECT channel formation again show a distinct difference between pure ETE-PC and the ETE-S-containing samples (Figure 5b). As observed in

© 2024 The Author(s). Advanced Electronic Materials published by Wiley-VCH GmbH

2199160x, 2025, 17, Downloaded from https://advanced.onlinelibrary.wiley.com/doi/10.1002/aelm.202400681 by Statens Beredning, Wiley Online Library on [30/10/2025]. See the Terms and Conditions (https://onlinelibrary.wiley.com/terms-and-conditions) on Wiley Online Library for rules of use; OA articles are governed by the applicable Creative Commons License

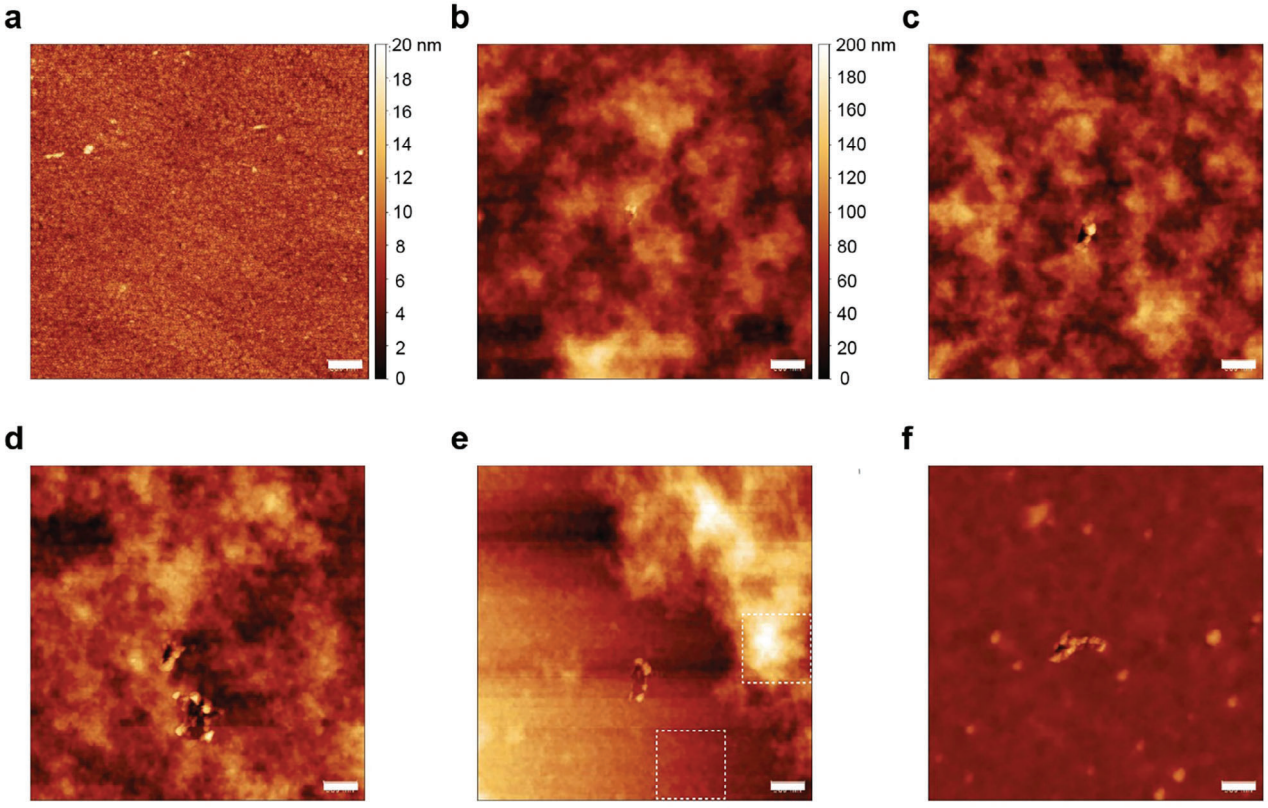

Figure 4. AFM images at the central region of dried EQCM-D Au/Ti quartz sensors showing height information for a) bare Au, and electropolymerized b) ETE-S 100%, c) ETE-S:PC 75:25, d) ETE-S:PC 50:50, e) ETE-S:PC 25:75, and f) ETE-PC 100%; 5 μm^2 scan size and 500 nm scale bar for all images, common color scale for all images except the first.

the QCM-D data, ETE-S-containing samples exhibit a higher initial growth rate but show signs of saturation within the 60 s electropolymerization timeframe (Figure 3b–d). This is again likely due to the electromigration of ETE-S toward the positively charged source electrode and the thickness limit imposed by the negative charge of the deposited polymer. In contrast, the charge-balanced ETE-PC requires more time to bridge the gap and is furthest from saturation. Aside from the ETE-S sample, the current reached at the end of electropolymerization correlates with the adsorbed mass (or thickness) of the electropolymerized film as determined by QCM-D (Table S1, Supporting Information), which can be expected of a material where the entire bulk participates in ionic and electronic conduction.

Table 1. Surface roughness values for each image are shown in Figure 4.

ETE-S:PC	RMS roughness [nm]
0:0 (bare Au)	1.46
100:0	24.24
75:25	21.93
50:50	22.72
25:75	34.69*)
0:100	6.03

*) Average roughness over the entire image. Local RMS roughness ranges from 7.87 nm in the apparently smoother region (bottom) to 37.61 nm in the rougher region (middle), indicated by the ≈1 μm^2 dotted white squares in Figure 4e.

To assess the effects of the monomer composition on the threshold voltage of the resulting polymers, the monomer solution is replaced by 0.01 M NaCl electrolyte, whereupon the transfer curves are collected at a fixed drain voltage V_d of −0.4 V and a varying the gate voltage V_g in the range of +0.6– −0.8 V (Figure 5c). As seen in Figure 5d, the normalized transfer curve of the OECT shifts toward positive voltages with increased proportions of ETE-S, indicating a higher native doping level in the absence of applied gate voltage with higher proportions of ETE-S. The gradual transition in the transfer characteristics indicates that, like the monomer aggregates, the polymer material is uniform and displays properties proportional to the weighted average of its components. While the normalized transfer curves exhibit very little variance among trials, raw current values of the transfer curves do not correlate with the trend observed during electropolymerization and have very large standard deviations (Figure S6b, Supporting Information). This effect is attributed to the inefficient removal of entrapped monomers from the polymer film. A protocol to remove excess monomer that is embedded in the polymer channel is expected to improve the channel conductance and reproducibility of these devices.

In general, aggregation effects are rarely considered during electropolymerization of conducting polymers because the best

 © 2024 The Author(s). Advanced Electronic Materials published by Wiley-VCH GmbH

2199160x, 2025, 17, Downloaded from https://advanced.onlinelibrary.wiley.com/doi/10.1002/aelm.202400681 by Statens Beredning, Wiley Online Library on [30/10/2025]. See the Terms and Conditions (https://onlinelibrary.wiley.com/terms-and-conditions) on Wiley Online Library for rules of use; OA articles are governed by the applicable Creative Commons License

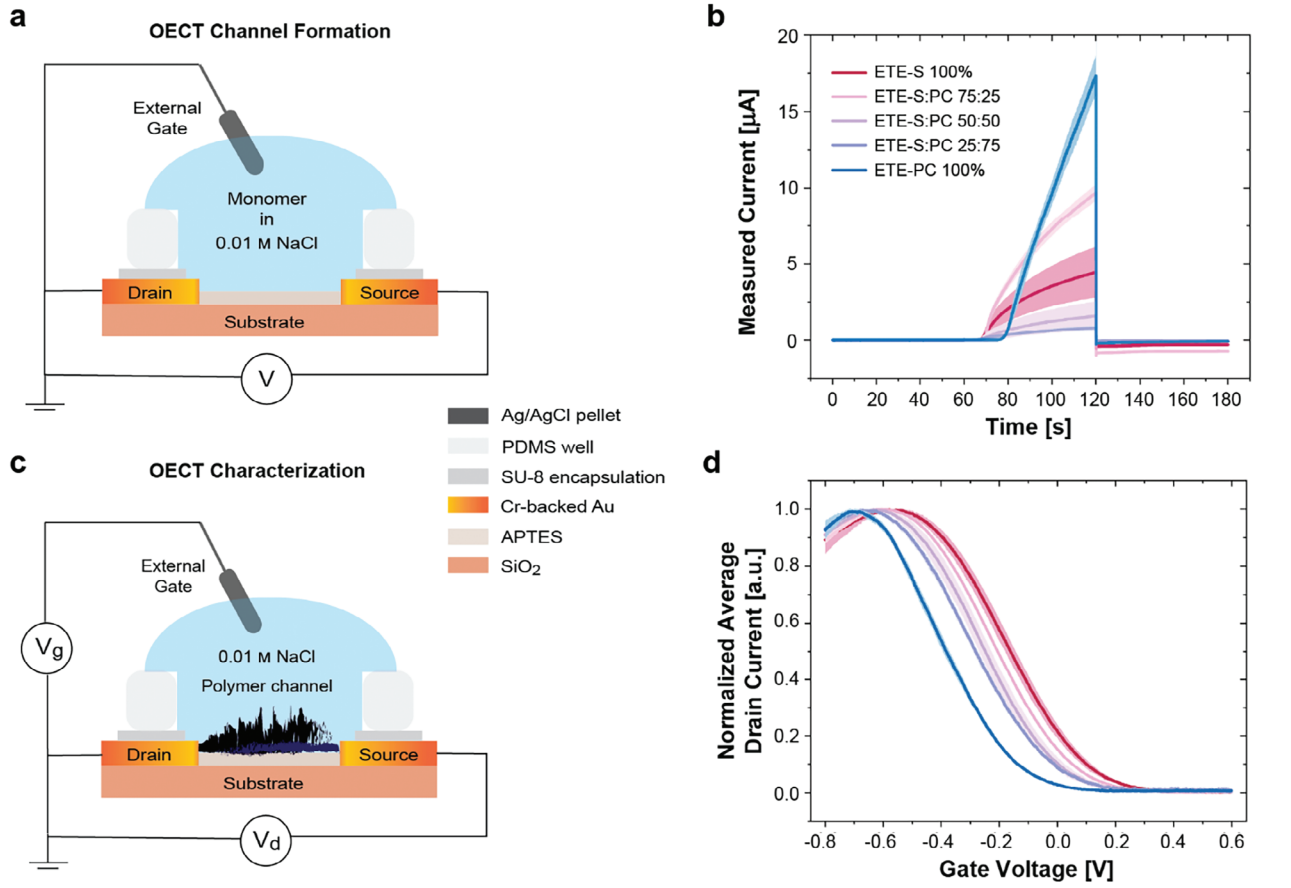

Figure 5. Schematics depicting the structure of a sample OECT device along with the corresponding circuit connections used for a) channel formation and c) transfer characteristics measurements; OECT measurements consisting of b) measured output current overtime during the three-minute CA procedure to grow the polymer channels, along with d) measured output current vs applied input voltage for the five samples; error bars represent standard deviation calculated from at least four device channels per sample.

practice for setting up an experiment is to choose a solvent in which the monomers are well-dissolved. Nevertheless, aggregation is shown to impact the electropolymerization process and the properties of the films thus formed in this work. Some indicators of the significance of aggregation exist in the literature. There has been extensive evidence that adding a small quantity of bad solvent improves the properties of electropolymerized polythiophene (PTh) and polypyrrole (PPy) films.[25–28] The accepted theory is that water acts as a base that helps extract the protons in the deprotonation step, but this effect could also potentially be due to water-promoting monomer aggregation, which reduces the spacing between monomers and increases the likelihood of two electrogenerated radicals encountering one another within their lifetime. Here, it is shown that rather than being an undesirable effect, aggregation can be exploited to fine-tune the properties of devices fabricated by electropolymerization.

3. Conclusion

Here, the aggregation of heterogeneous monomers is exploited to fine-tune both the electropolymerization parameters and the properties of OECT devices fabricated by electropolymerization. Monomers with a common ETE backbone, but differing sidechains, are found to form aggregates with homogeneous distributions, exhibiting properties that are roughly a weighted average of their constituents. Spectroscopic and structural analyses indicate that ETE-S, the anionic monomer, exhibits higher degrees of backbone stacking and produces 2D nanoscale aggregates, presumably due to the dominance of sidechain repulsion in its intermolecular interactions. The π–π stacking is less prominent in ETE-PC aggregates, which have the morphology of circular beads on a string. Electrochemical evaluation of the electropolymerization onset shows that blends of ETE-S and -PC mostly behave as uniform amalgams rather than maintaining the characteristics of their separate entities. Likewise, the threshold voltage of OECTs produced by electropolymerization of the monomer blends changes continuously in accordance with the monomer ratio. This simple approach to fine-tune device properties can serve as a significant advantage in building circuits with electropolymerized OECTs.

4. Experimental Section

In this study, monomer solutions of ETE-S and ETE-PC at various relative concentrations were investigated; each at a concentration of 0.001 M in

© 2024 The Author(s). Advanced Electronic Materials published by Wiley-VCH GmbH

2199160x, 2025, 17, Downloaded from https://advanced.onlinelibrary.wiley.com/doi/10.1002/aelm.202400681 by Statens Beredning, Wiley Online Library on [30/10/2025]. See the Terms and Conditions (https://onlinelibrary.wiley.com/terms-and-conditions) on Wiley Online Library for rules of use; OA articles are governed by the applicable Creative Commons License

0.01 M NaCl electrolyte used as was, and also mixed together at ratios of 75% and 25%, 50% and 50%, and 25% and 75%, respectively, to get corresponding five sample solutions: ETE-S 100%, ETE-S:PC 75:25, ETE-S:PC 50:50, ETE-S:PC 25:75, and ETE-PC 100%. Varying aggregation behavior was observed using UV–vis spectroscopy. The monomer samples were also electropolymerized in situ and monitored via electrochemical quartz crystal microbalance with dissipation (EQCM-D) to simultaneously determine the polymerization onset potential along with the mass and viscoelastic properties of the resulting polymer films. These films were further characterized using atomic force microscopy (AFM). The five ETE-X blends were electropolymerized between the pre-patterned source and drain electrodes to form OECTs. Lastly, three of the five monomer solutions i.e., pure ETE-S and ETE-PC, along with their 50:50 mix, were observed through dynamic light scattering (DLS) and liquid phase transmission electron microscopy (LPTEM) to determine the size and appearance of these monomer aggregates in aqueous NaCl, as well as through scanning electron microscopy (SEM) for dried monomer aggregate samples.

Chemical Synthesis: ETE-S and ETE-PC were synthesized as previously published.[10,29] Fabrication of OECT devices along with surface modification using (3-aminopropyl) triethoxysilane (APTES, Sigma–Aldrich), were also carried out as previously published.[10,29,30] The common electrolyte for all measurements and sample preparations was 0.01 M NaCl (Sigma–Aldrich) in deionized (DI) water.

UV-Visible Spectroscopy: Absorbance spectra of the monomer solutions were obtained using a Synergy H1 microplate reader (Bio-Tek) for 100 µL sample volumes at room temperature in a polypropylene 96-well F-bottom clear microplate (Greiner Bio-One). After a linear shake of 1 min, wavelengths were scanned from 300 to 999 nm at 1 nm per step and three reads per microplate well were measured and subtracted from corresponding data for 0.01 M NaCl, to determine the average UV–vis spectra of the five monomer samples. Similarly, fluorescence emission spectra for the samples were also obtained for excitation wavelengths of 350 and 450 nm, and corresponding scan ranges of excitation+50 to 700 nm at 1 nm per step and three reads per microplate well.

EQCM-D: EQCM-D measurements were carried out using a QSense E4 Analyzer (Biolin Scientific), an integrated pneumatic control (IPC) high-precision multichannel pump (ISMATEC), and a µAutolab III potentiostat (Metrohm). The 3-electrode setup consisted of Au/Ti coated quartz sensor (5 MHz, Biolin Scientific) as the working electrode, Pt plate (Biolin Scientific) of the EQCM-D module as the counter electrode, and an external Dri-Ref Ag/AgCl (World Precision Instruments) as the reference electrode. EQCM-D sensors were cleaned by immersing them in a cleaning solution (DI water, 31% H_2O_2, and 25% NH_4OH mixed in a ratio of 5:1:1) for 7 min at 100 °C, rinsing using DI water, drying using N_2 stream, then UV-Ozone (Novascan Technologies) cleaning for 30 min. Cyclic voltammetry (CV) and chronoamperometry (CA) measurements were performed using a single junction Ag/AgCl electrode (3 M KCl) as a reference. A 0.1 V s^{-1} scan rate was used for the CV measurements, and a 0.01 s interval time was used for the CA measurements. Results were obtained and analyzed using QSoft, QTools, QSense Dfind 1.2.7, Nova 2.1, and Origin 2024 software.

Device Fabrication and Characterization: OECT devices made up of Cr-backed Au electrodes microfabricated on a silicon wafer with a 1 µm thick thermally deposited oxide layer (Silicon Valley Microelectronics) and surface-modified with APTES treatment as per published protocol,[30] were characterized using a Keithley 2612B SourceMeter, with a polydimethylsiloxane (PDMS) well. The devices were structured as a 46-channel array of input contacts that could be addressed independently, and a common output contact that was used as the ground in all experiments ($W = 100$ µm, $L = 10$ µm). Within the well, there was also a 1×2 mm^2 Au/Cr electrode that was used to measure the onset potential of the monomer by CV before each set of electropolymerization experiments relative to an E-206 Ag/AgCl pellet (Science Products) reference electrode. OECT channels were then grown between the chosen device drain and source electrodes by applying the corresponding electropolymerization onset potential plus a common offset potential of 0.2 V for 1 min, between the independently addressed input electrode and the Ag/AgCl reference electrode that was shorted with the common output electrode and grounded. A potential of −0.05 V was also applied for 1 min before and after this channel growth step. After each set of depositions on a single device, the sample was rinsed once with 300 µL of aqueous 0.01 M NaCl, then replaced with fresh 300 µL of the same electrolyte solution to obtain the transfer curves for the electropolymerized channels. Transfer data for the OECTs were acquired at a fixed drain voltage of −0.4 V and a gate voltage within the range of +0.6 to −0.8 V at 0.05 V s^{-1} scan rate.

AFM (Atomic Force Microscopy): Polymer-coated substrates formed during EQCM-D measurements were dried under ambient conditions and observed under a Dimension Icon XR (Bruker) instrument, using ScanAsyst-Air cantilever operating in ScanAsyst-Air mode. Images were acquired using Nanoscope v10 and analyzed using Gwyddion 2.65 after basic operations like correcting horizontal scars, levelling data by mean plane subtraction, aligning rows using median method, and shifting minimum data value to zero.

DLS (Dynamic Light Scattering): Monomer samples of ETE-S 100%, ETE-PC 100%, and ETE-S:PC 50:50 mix, each at a concentration of 0.001 M in 0.01 M NaCl electrolyte, were observed using Zetasizer Nano ZS90 (Malvern Panalytical) fitted with a 4 mW 632.8 nm laser. UV-transparent disposable polystyrene cuvettes with cap (Sarstedt) containing 100 µL of the sample were measured at 22 °C. The selected settings were material as protein, dispersant as water, equilibration time of 60 s, and scattering detector angle of 90° in the Zetasizer Software v. 8.02. The average size distribution was obtained using data from 3 measurements per sample, with a total of 100 runs of 10 s each per measurement, and processed using general purpose analysis model.

LPTEM (Liquid Phase Transmission Electron Microscopy): Monomer samples of ETE-S 100%, ETE-PC 100%, and ETE-S:PC 50:50 mix, each at a concentration of 0.005 M in 0.01 M NaCl electrolyte were imaged by bright-field TEM at 300 KV using Titan 80–300 (FEI Company) instrument. A stream liquid biasing holder (DENSsolutions) containing 0.6 µL of the drop-cast sample in the nano-cell was introduced into the microscope. This closed-cell system enabled in situ visualization of liquid samples in the high vacuum ($\approx 10^{-5}$ Pa) TEM environment.

SEM (Scanning Electron Microscopy): Monomer samples from LPTEM experiments were dried by opening the Nano-Cell and allowing the solution to evaporate at ambient conditions. The dried monomer samples were then imaged using a JEOL 7800F Prime instrument at an acceleration voltage of 1 KV and high vacuum ($\approx 10^{-5}$ Pa) conditions. Information about the morphology of the dried monomer aggregates was obtained using secondary electron imaging.

Supporting Information

Supporting Information is available from the Wiley Online Library or from the author.

Acknowledgements

The authors would like to thank Benjamin Granroth, Marios Savvakis, Bernhard Burtscher, and Dr. Deyu Tu for informative discussions and knowledge-sharing that helped shape this work. This work was supported by the Swedish Foundation for Strategic Research (RMX18-0083), the Swedish Research Council (2018–06197), and the European Research Council (834677 e-NeuroPharma ERC-2018-ADG). Additional support was provided by the Knut and Alice Wallenberg Foundation. This work was performed in part at the Chalmers Materials Analysis Laboratory (CMAL).

Conflict of Interest

The authors declare no conflict of interest.

Data Availability Statement

The data that support the findings of this study are available from the corresponding author upon reasonable request.

© 2024 The Author(s). Advanced Electronic Materials published by Wiley-VCH GmbH

2199160x, 2025, 17, Downloaded from https://advanced.onlinelibrary.wiley.com/doi/10.1002/aelm.202400681 by Statens Beredning, Wiley Online Library on [30/10/2025]. See the Terms and Conditions (https://onlinelibrary.wiley.com/terms-and-conditions) on Wiley Online Library for rules of use; OA articles are governed by the applicable Creative Commons License

Keywords

aggregation, conducting polymer, electropolymerization, organic electrochemical transistor (OECT), threshold voltage

Received: August 28, 2024
Revised: October 7, 2024
Published online: November 22, 2024

[1] K. Myny, *Nat. Electron.* **2018**, *1*, 30.
[2] R. A. Street, T. N. Ng, D. E. Schwartz, G. L. Whiting, J. P. Lu, R. D. Bringans, J. Veres, *Proc IEEE* **2015**, *103*, 607.
[3] S. E. Doris, A. Pierre, R. A. Street, *Adv. Mater.* **2018**, *30*, 1706757.
[4] S. T. M. Tan, G. Lee, I. Denti, G. LeCroy, K. Rozylowicz, A. Marks, S. Griggs, I. McCulloch, A. Giovannitti, A. Salleo, *Adv. Mater.* **2022**, *34*, 2202359.
[5] H. Tseng, A. Weissbach, J. Kucinski, A. Solgi, R. Nair, L. M. Bongartz, G. Ciccone, M. Cucchi, K. Leo, H. Kleemann, *Adv. Mater. Interfaces* **2023**, *10*, 2201914.
[6] V. Kaphle, P. R. Paudel, D. Dahal, R. K. Radha Krishnan, B. Lüssem, *Nat. Commun.* **2020**, *11*, 2515.
[7] M. Cucchi, A. Weissbach, L. M. Bongartz, R. Kantelberg, H. Tseng, H. Kleemann, K. Leo, *Nat. Commun.* **2022**, *13*, 4514.
[8] C. Zhang, Y. Xu, N. Wang, Y. Xu, W. Xiang, M. Ouyang, C. Ma, *Electrochim. Acta* **2009**, *55*, 13.
[9] M. Balkhandia, R. Kedia, M. Khatak, N. Chaudhary, A. Patra, *Electrochim. Acta* **2023**, *466*, 143002.
[10] J. Y. Gerasimov, A. Halder, A. H. Mousa, S. Ghosh, P. C. Harikesh, T. Abrahamsson, D. Bliman, J. Strandberg, M. Massetti, I. Zozoulenko, D. T. Simon, M. Berggren, R. Olsson, S. Fabiano, *Adv. Funct. Mater.* **2022**, *32*, 2202292.
[11] I. Sahalianov, T. Abrahamsson, D. Priyadarshini, A. H. Mousa, K. Arja, J. Y. Gerasimov, M. Linares, D. T. Simon, R. Olsson, G. Baryshnikov, M. Berggren, C. Musumeci, *J. Phys. Chem.* **2024**, *128*, 6581.
[12] M. Kim, J. Choi, S. Y. Kim, *Mater. Today Chem.* **2022**, *26*, 101014.
[13] P. Chapagain, G. Guisbiers, M. Kusper, L. D. Geoffrion, M. Benamara, A. Golden, A. Bachri, L. Hewavitharana, *ACS Omega* **2021**, *6*, 6871.
[14] E. L. Lyngdoh, V. Nayan, M. Vashisht, S. Kumari, A. Bhardwaj, T. Bhatia, J. Dalal, S. Pawaria, S. K. Onteru, P. Sikka, D. Singh, *Biotechnol. Lett.* **2020**, *42*, 1383.
[15] S. Rathnakumar, S. Bhaskar, V. Sivaramakrishnan, N. S. V. Kambhampati, V. Srinivasan, S. S. Ramamurthy, *Anal. Chem.* **2024**, *96*, 4005.
[16] D. Priyadarshini, C. Musumeci, D. Bliman, T. Abrahamsson, C. Lindholm, M. Vagin, X. Strakosas, R. Olsson, M. Berggren, J. Y. Gerasimov, D. T. Simon, *Langmuir* **2023**, *39*, 8196.
[17] G. A. McCubbin, S. Praporski, S. Piantavigna, D. Knappe, R. Hoffmann, J. H. Bowie, F. Separovic, L. L. Martin, *Eur. Biophys. J.* **2011**, *40*, 437.
[18] MedCalc's Comparison of Means Calculator, https://www.medcalc.org/calc/comparison_of_means.php (accessed: August 2024).
[19] I. Reviakine, D. Johannsmann, R. P. Richter, *Anal. Chem.* **2011**, *83*, 8838.
[20] A. D. Easley, T. Ma, C. I. Eneh, J. Yun, R. M. Thakur, J. L. Lutkenhaus, *J. Polym. Sci.* **2022**, *60*, 1090.
[21] S. Sharma, P. Chand, *Results Chem.* **2023**, *5*, 100885.
[22] L. E. Helseth, *J. Energy Storage* **2021**, *35*, 102304.
[23] N. Parveen, P. K. Jana, M. Schönhoff, *Polymer* **2019**, *11*, 1285.
[24] R. P. Richter, K. B. Rodenhausen, N. B. Eisele, M. Schubert, in *Coupling Spectroscopic Ellipsometry and Quartz Crystal Microbalance to Study Organic Films at the Solid-Liquid Interface* (Eds: K. Hinrichs, K. J. Eichhorn), Ellipsometry of Functional Organic Surfaces and Films. Springer Series in Surface Sciences, Springer, Cham **2018**, Vol *52*, pp. 225–246.
[25] J. Heinze, B. A. Frontana-Uribe, S. Ludwigs, *Chem. Rev.* **2010**, *110*, 4724.
[26] F. Beck, M. Oberst, R. Jansen, *Electrochim. Acta* **1990**, *35*, 1841.
[27] A. J. Downard, D. Pletcher, *J. Electroanal. Chem. Interfacial Electrochem.* **1986**, *206*, 139.
[28] T. Costa, D. De Azevedo, B. Stewart, M. Knaapila, A. J. M. Valente, M. Kraft, U. Scherf, H. D. Burrows, *Polym. Chem.* **2015**, *6*, 8036.
[29] J. Y. Gerasimov, D. Zhao, A. Sultana, T. Abrahamsson, S. Han, D. Bliman, D. Tu, D. T. Simon, R. Olsson, X. Crispin, M. Berggren, S. Fabiano, J. Y. Gerasimov, D. Zhao, A. Sultana, T. Abrahamsson, S. Han, D. Tu, D. T. Simon, X. Crispin, M. Berggren, S. Fabiano, D. Bliman, R. Olsson, *Adv. Electron. Mater.* **2021**, *7*, 2001126.
[30] J. Y. Gerasimov, D. Tu, V. Hitaishi, C. Harikesh, C.-Y. Yang, T. Abrahamsson, M. Rad, M. J. Donahue, S. Ejneby, M. Berggren, R. Forchheimer, S. Fabiano, J. Y. Gerasimov, D. Tu, V. Hitaishi, P. C. Harikesh, C.-Y. Yang, T. Abrahamsson, M. Rad, M. J. Donahue, M. Berggren, S. Fabiano, M. S. Ejneby, R. Forchheimer, *Adv. Sci.* **2023**, *10*, 2207023.

© 2024 The Author(s). Advanced Electronic Materials published by Wiley-VCH GmbH

2199160x, 2025, 17, Downloaded from https://advanced.onlinelibrary.wiley.com/doi/10.1002/aelm.202400681 by Statens Beredning, Wiley Online Library on [30/10/2025]. See the Terms and Conditions (https://onlinelibrary.wiley.com/terms-and-conditions) on Wiley Online Library for rules of use; OA articles are governed by the applicable Creative Commons License